Ferrite-guided cyclotron-resonance maser

Eli Jerby,* A. Kesar, A. Aharony, and G. Breitmeier
Faculty of Engineering, Tel Aviv University, Ramat Aviv 69978, Israel
(Received 15 May 2001; revised manuscript received 20 February 2002; published 10 June 2002)

The concept of a cyclotron-resonance maser (CRM) with a ferrite loading incorporated in its waveguide is proposed. The CRM interaction occurs between the rotating electron beam and the em wave propagating along a longitudinally magnetized ferrite medium. The ferrite anisotropic permeability resembles the CRM susceptibility in many aspects, and particularly in their similar response to the axial magnetic field (the ferrite susceptibility can be regarded as a passive analog of the active CRM interaction). The ferrite loading slows down the phase velocity of the em wave and thus the axial (Weibel) mechanism of the CRM interaction dominates. The ferrite loading enables also a mechanism of spectral tunability for CRM's. The ferrite loading is proposed, therefore, as a useful ingredient for high-power CRM devices. A linear model of the combined ferrite-guided CRM interaction reveals its useful features. Future schemes may also incorporate ferrite sections functioning as isolators, gyrators, or phase shifters within the CRM device itself for selective suppression of backward waves and spurious oscillations, and for gain and efficiency enhancement.

DOI: 10.1103/PhysRevE.65.066502 PACS number(s): 52.59.Px, 84.40.Ik, 84.40.Az

I. INTRODUCTION

Cyclotron resonance masers (CRM's) are well-known sources of high-power microwaves and millimeter waves [1]. Two competing physical mechanisms are involved in the interaction of the em wave with the helical orbiting electron beam in the axial magnetic field [2]. The first mechanism originates from the relativistic dependence of the cyclotron frequency on the electron energy. This effect induces azimuthal phase bunching of the orbiting electrons. The opposite mechanism is the axial bunching effect caused by the axial velocity modulation of the electrons (this effect is also known as the Weibel interaction).

The azimuthal bunching mechanism dominates in fast-wave devices. For instance, gyrotron devices [3] utilize highly azimuthal bunching due to their large em phase velocity (near the waveguide cutoff). Gyrotrons have recently reached up to an 850 GHz frequency [4] and up to a 70 dB amplifier gain [5]. The latter achievement is made feasible by a distributed loss along the interaction, which suppresses the undesired backward waves.

The axial bunching mechanism dominates in slow-wave CRM's. Such devices, with dielectric loads [6,7] and periodic waveguides [8,9], have been demonstrated experimentally. The dielectric load or the periodic structure (i.e., artificial dielectric) decreases the impedance of the em wave involved in the azimuthal bunching, and enhances the opposite axial bunching effect, which may then dominate. The anomalous Doppler CRM effect [7,10,11] may occur in these conditions. This effect, for instance, enables amplification even with a zero initial transverse velocity component of the electrons [12]. This feature alleviates the need for an initial kicking of the electron beam, and it may simplify the CRM device operating in the anomalous regime.

This paper proposes the concept of a CRM interaction incorporated in a ferrite-loaded waveguide [13]. Ferrite loads were discussed already in the early 1960s for backward-wave tubes [14,15]. In the presently proposed CRM, the ferrite loading slows down the wave phase velocity and enhances the magnetic field component of the em wave involved in the axial bunching effect. Unlike periodic or dielectric loads for slow-wave CRM's, the ferrite permeability is a resonant effect governed by the same axial (static) magnetic field incorporated in the CRM device itself. The linear model presented in this paper shows that the ferrite loading may provide an additional tunability feature of the CRM interaction since the waveguide spectral response is tuned simultaneously with the CRM interaction by the static magnetic field.

Ferrite-guided CRM's can be conceived in a variety of different schemes. In this paper we study a cylindrical metallic waveguide loaded by a hollow ferrite rod as shown in Fig. 1 (other structures based on rectangular or planar waveguides are feasible as well). In the scheme shown in Fig. 1, an axial magnetic field is applied externally to activate both the CRM interaction and the ferrite anisotropic permeability.

Ferrite materials are used in a wide range of passive non-

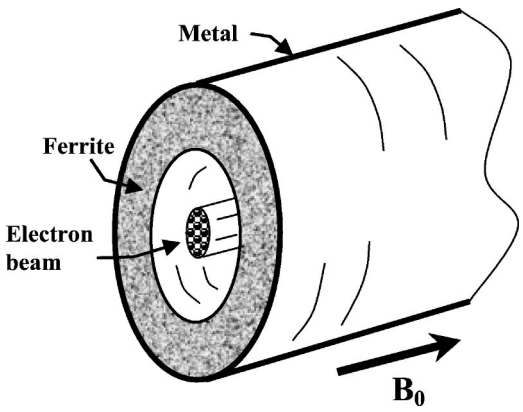

FIG. 1. The proposed ferrite-guided CRM scheme in a cylindrical waveguide.

*Author to whom correspondence should be addressed. Electronic address: jerby@eng.tau.ac.il

reciprocal microwave devices, such as isolators, gyrators, circulators, filters, and phase shifters [16,17]. Hence, these functions can be incorporated as well in future CRM schemes. For instance, one may conceive an ''isolator CRM'' in which the backward waves or other spurious oscillations are suppressed selectively by the ferrite. The amplified forward wave will not be attenuated then as in [5], since the resonance frequencies of the ferrite loss and of the forward CRM interaction deviate by the Doppler shift. Ferrite elements can be conceived also for phase shifting within the CRM interaction, to enhance its gain and efficiency.

This paper is organized as follows. Section II presents a transverse-mode analysis for the cylindrical ferrite-loaded waveguide shown in Fig. 1, and a linear gain-dispersion relation of the corresponding CRM interaction. Section III introduces the extended tunability feature of a ferrite-loaded CRM, and Sec. IV summarizes the paper and proposes directions for future ferrite-guided CRM studies.

II. LINEAR MODEL

The linear model derived in this section demonstrates physical features of the ferrite-guided CRM. This model assumes an electron beam spiraling in a uniform magnetic field along a hole in the cylindrical ferrite-loaded waveguide illustrated in Fig. 1. This model presents the features of the device and can be generalized to other schemes as well. The em wave propagating on the z axis along with the electron beam is tuned to the range of a single circularly polarized waveguide mode. Section II A analyzes the transverse effects of the bounded ferrite medium on the guided em wave. This results in mode dispersion and impedance, and the e-beam filling-factor parameters. These constitutive parameters are incorporated in Sec. II B in the kinetic linear model derived for the convective cyclotron instability. This approach enables us to focus first on the principal contribution of the ferrite guide to the CRM interaction.

In view of the CRM scheme shown in Fig. 1, we obtain from Maxwell's equations a tensor wave equation as follows:

$$\nabla^2\mathbf{H}+\omega^2\varepsilon\underline{\underline{\mu}}\mathbf{H}=\begin{cases}-\nabla\times\mathbf{J}, & 0<r<r_b\\ \mathbf{0}, & r_b<r<R_o,\end{cases} \tag{1}$$

where $\mathbf{H}$ is the magnetic field component of the em wave, ε is the (nonuniform) effective dielectric permitivity of the medium, ω is the em wave angular frequency, $\mathbf{J}$ and r_b are the electron-beam current and radius, respectively (assuming a pencil e beam), and R_o is the inner radius of the metallic waveguide. The permeability tensor is given for the ferrite medium by [16]

$$\underline{\underline{\mu}}=\mu_0\begin{pmatrix}\mu_r & -j\kappa_r & 0\\ j\kappa_r & \mu_r & 0\\ 0 & 0 & 1\end{pmatrix}, \tag{2}$$

where the scalar permeability terms, neglecting losses, are

$$\mu_r=1-\frac{\omega_0\omega_M}{\omega^2-\omega_0^2}, \tag{3a}$$

$$\kappa_r=\frac{\omega\omega_M}{\omega^2-\omega_0^2}. \tag{3b}$$

In vacuum, the permeability tensor $\underline{\underline{\mu}}$ is reduced to μ_0. The ferrite resonance and the magnetization angular frequencies are given by

$$\omega_0=\frac{e}{m_0}\mu_0 H_i, \tag{4a}$$

$$\omega_M=\frac{e}{m_0}\mu_0 M_i, \tag{4b}$$

respectively; both resemble the cyclotron angular frequency in the magnetized electron beam

$$\omega_{c0}=\frac{e}{m_0}B_0, \tag{5}$$

where e and m_0 are the electron charge and rest mass, respectively, H_i is the static magnetic induction inside the ferrite and M_i is its magnetization, and B_0 is the static magnetic field induced on the electron beam. The em-wave modes propagating in a magnetized ferrite medium are inherently circularly polarized waves [16,17]. Their relative permeability $\mu_{r\pm}=\mu_r\pm\kappa_r$ depends on frequency. The effect of the metallic bound is elaborated in the next section.

A. The ferrite-loaded cylindrical waveguide

The modes of em-wave propagation in a cylindrical waveguide partially filled with a ferrite tube (without an electron beam) were investigated by Baden-Fuller [18]. In this study he derived a comprehensive model for the dispersion relation and the transverse profiles of these waveguide modes. In this model, the homogeneous tensor wave equation [Eq. (1) with $\mathbf{J}=\mathbf{0}$] for the waveguide shown in Fig. 1 leads to the coupled wave equation for the transverse and axial wave components as follows:

$$\mu_r\nabla_\perp^2 H_z+(\omega^2\varepsilon\mu_0\mu_r-\beta^2)H_z=j\omega\varepsilon\beta\kappa_r E_z, \tag{6a}$$

$$\mu_r\nabla_\perp^2 E_z+[\omega^2\varepsilon\mu_0(\mu_r^2-\kappa_r^2)-\mu_r\beta^2]E_z = -j\omega\mu_0\beta\kappa_r H_z, \tag{6b}$$

where β is the longitudinal wave number, and E_z and H_z are the longitudinal electric and magnetic field components. The ferrite-loaded cylindrical waveguide supports composite em wave modes, which cannot be classified as pure TE or TM modes like the empty waveguide modes. Hence, these modes possess both longitudinal E_z and H_z components due to the nonisotropic ferrite properties represented by the κ_r term in Eqs. (2), (6a), and (6b).

The waveguide modes are found in Ref. [18] by a sixth-order matrix dispersion equation of the form $\underline{\underline{\mathbf{D}}}(\beta)\underline{\mathbf{L}}=0$ ob-

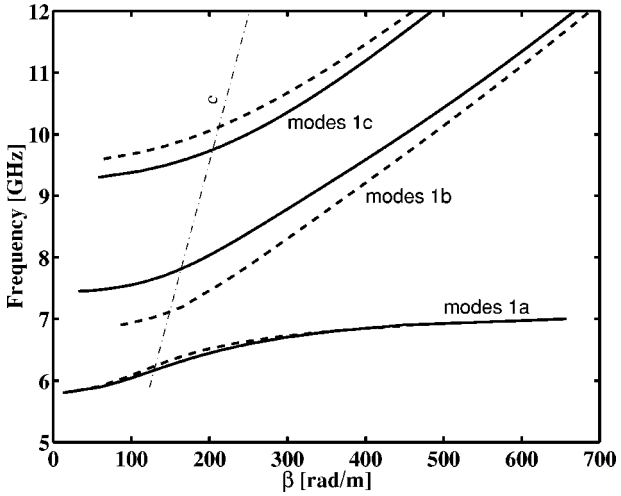

FIG. 2. Computed dispersion relations of the first three modes in a ferrite-loaded cylindrical waveguide. The waveguide parameters are listed in Table I. The external magnetization field $B_0=2.5$ kG. The solid and dashed lines describe the right-hand (R) and left-hand (L) circular polarization modes, respectively. The free-space slope of c is also shown for comparison.

tained by applying boundary conditions to the general solution of Eqs. (6a) and (6b) on the inner and outer ferrite jacket surfaces. The β-dependent terms of the sixth-order matrix $\underline{\underline{\mathbf{D}}}$ are listed in [18]. The solution of the vector $\underline{\mathbf{L}}$ provides the coefficients for the em-wave components in the vacuum and ferrite media, as calculated below. The dispersion relation $\beta(\omega)$ of the ferrite-loaded waveguide modes is found by the numerical solutions of $\det\underline{\underline{\mathbf{D}}}(\beta)=0$. Figure 2 shows the computed dispersion relations for the left- and right-hand circularly polarized modes of the first three modes for the parameters listed in Table I.

Reference [18] presents general expressions for the various field components. These include the transverse magnetic field components in the waveguide bore region (i.e., the e-beam vicinity on axis) as follows:

$$H_r = Z_0^{-1}\left[\frac{2\pi}{\gamma_a^2}\frac{n}{\bar{r}}K_3 J_n(\gamma_a\bar{r}) - \bar{\beta}\frac{2\pi}{\gamma_a}K_4 J_n'(\gamma_a\bar{r})\right] \times e^{j(n\theta+\omega t-\beta z)}, \tag{7a}$$

TABLE I. Parameters for numerical calculations.

Parameter	Symbol	Value
Ferrite-loaded cylindrical waveguide		
Length	L	1 m
Ferrite inner/outer radius	R_i/R_o	5/8 mm
Relative dielectric factor	ε_r	12.9
Maximum magnetization	$4\pi\mu_0 M_i$	3 kG
Electron beam		
Current	I	1 A
Voltage	V_{eb}	6–9 kV
Beam radius	r_b	2 mm
Pitch ratio	α	1

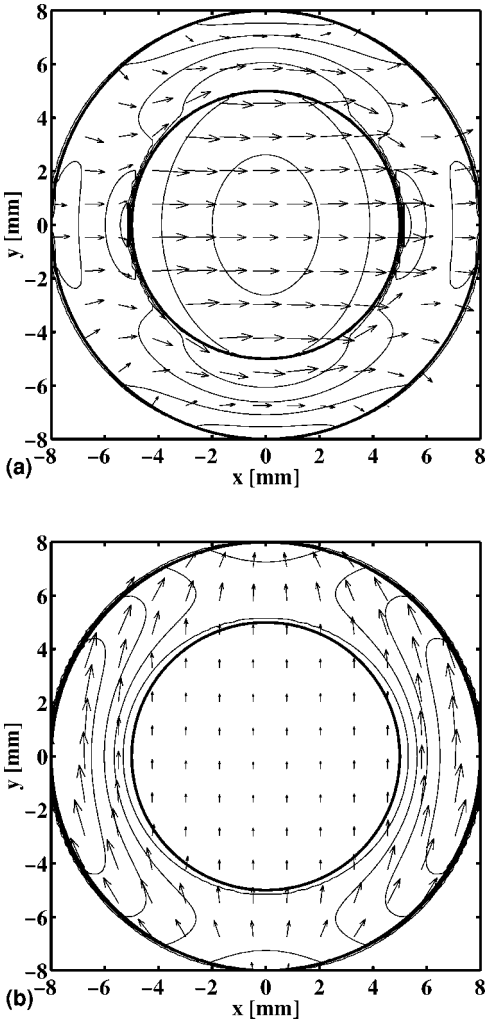

FIG. 3. Computed transverse profiles of the electric (a) and magnetic (b) vector fields, and their corresponding intensity contours, across the partially filled ferrite loaded waveguide (without an e beam), for the right-hand circularly polarized mode denoted "1b" in Fig. 2 at a frequency of 9 GHz and $B_0=2.5$ kG.

$$H_\theta = jZ_0^{-1}\left[-\frac{2\pi}{\gamma_a^2}\bar{\beta}\frac{n}{\bar{r}}K_4 J_n(\gamma_a\bar{r}) + \frac{2\pi}{\gamma_a}K_3 J_n'(\gamma_a\bar{r})\right] \times e^{j(n\theta+\omega t-\beta z)}, \tag{7b}$$

where $Z_0=\sqrt{\mu_0/\varepsilon_0}$ is the free-space wave impedance, K_3 and K_4 are coefficients resulting numerically from the vector $\underline{\mathbf{L}}$ solution, $\bar{r}=r/\lambda_0$ and $\bar{\beta}=\beta/k_0$ are the radial coordinate and the axial wave number, respectively (normalized to the free-space wavelength and wave number), $\gamma_a=2\pi\sqrt{1-\bar{\beta}^2}$, and n is the azimuthal index of the mode. Unlike in uniform waveguides, discrete radial indices are not valid for the partially filled ferrite waveguide. The mode presented by Eqs. (7a) and (7b) is inherently circularly polarized.

The em-wave profiles and the dispersion relations for the fundamental mode ($n=1$) are computed here by the Baden-Fuller model [18] for the parameters listed in Table I. Figure 3 presents the resulting profiles of the transverse em-wave

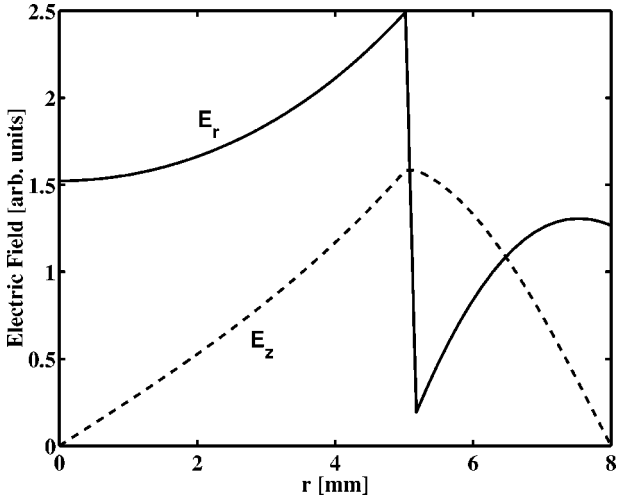

FIG. 4. The magnitude of the radial and axial electric field components $|E_r(r)|$ (solid line) and $|E_z(r)|$ (dashed line), respectively, of Fig. 3 along its horizontal axis.

components across the partially filled cylindrical ferrite waveguide for the right-hand circularly polarized mode (at $B_0=2.5$ kG, $\omega/2\pi=9$ GHz). Figure 4 shows the magnitude of the radial and axial electric field components ($|E_r(r)|$ and $|E_z(r)|$, respectively) along the horizontal axis of Fig. 3. The computed results show that near the waveguide axis the fundamental mode is dominated by the transverse field components. The wave profile is nearly uniform within the *e*-beam cross section ($r \leqslant r_b$), and it can be regarded there as a quasi-plane-wave. This circularly polarized quasi-plane-wave can be characterized near axis by its local impedance Z_a and wave number β. In the conditions of Fig. 3, these are found to be $Z_a=446\ \Omega$ and $\beta=327\ \mathrm{m}^{-1}$, respectively.

For a single-mode CRM interaction, the transverse effect of the waveguide is characterized also by the filling factor F_f which relates the effective cross-sectional areas of the *e* beam and the em mode as

$$F_f=\frac{A_{eb}}{A_{em}} \tag{8}$$

where $A_{eb}=\int_{\theta=0}^{2\pi}\int_{r=0}^{r_b}(\underline{\mathbf{S}}\cdot\hat{\mathbf{z}})r\,dr\,d\theta$ and

$$A_{em}=\int_{\theta=0}^{2\pi}\int_{r=0}^{R_o}(\underline{\mathbf{S}}\cdot\hat{\mathbf{z}})r\,dr\,d\theta,$$

and $\underline{\mathbf{S}}=\mathbf{E}\times\mathbf{H}^*$ is the Poynting vector of the em mode. The filling factor, impedance, and wave number of the em mode found above enable the derivation of the single-mode model for the ferrite-guided CRM interaction in the next section.

B. The cyclotron interaction

A linear model for the CRM interaction with a single waveguide mode is derived using the mode characteristics found above (i.e., the wave impedance, wave number, and filling factor parameters). Following Ref. [12], the electron current density is computed in the linear regime by

$$\mathbf{J}=-\frac{e}{m_0}\int\int\int_{\mathbf{P}_0}\frac{\mathbf{P}_c}{\gamma_0}f_{1c}(\mathbf{P}_0,z,\omega)d^3\mathbf{P}_0, \tag{9}$$

where $f_{1c}(\mathbf{P}_0,z,\omega)$ is the electron first-order distribution function, and $\mathbf{P}_c(\mathbf{P}_0)$ is the momentum characteristic line of the zero-order Vlasov equation. This line describes an electron spiraling trajectory along the axial magnetic field $\mathbf{B}_0=\hat{\mathbf{z}}B_0$, as

$$\mathbf{P}_c=\hat{\mathbf{x}}P_{0\perp}\cos\psi(z)+\hat{\mathbf{y}}P_{0\perp}\sin\psi(z)+\hat{\mathbf{z}}P_{0z}, \tag{10}$$

where $\psi(z)=k_c z+\psi_0$ is the phase of the electron gyromotion. The initial value of the momentum characteristic line is given in cylindrical coordinates by the initial components of the axial and radial electron momentum, P_{0z} and $P_{0\perp}$, respectively, and by the tilt angle α and the initial phase of the electron gyromotion, ψ_0. These are related to the Cartesian initial momentum components (P_{0x},P_{0y},P_{0z}) by $P_{0\perp}=\sqrt{P_{0x}^2+P_{0y}^2}$ and $\alpha=\arctan(P_{0y}/P_{0x})$, where both Cartesian and cylindrical coordinate systems are used simultaneously in the following analysis. The relativistic factor in Eq. (9) is given by $\gamma_0=\sqrt{1+(P_{0z}^2+P_{0\perp}^2)/m_0^2c^2}$ where c is the speed of light. The cyclotron motion periodicity in Eq. (10) is given by $k_c=\omega_c/V_{0z}$, where $V_{0z}=P_{0z}/\gamma_0 m_0$ is the initial axial velocity of the electron. The relativistic cyclotron frequency is $\omega_c=\omega_{c0}/\gamma_0$.

The first-order distribution function $f_{1c}(\mathbf{P}_0,z,\omega)$ in Eq. (9) is the solution of the first-order Vlasov equation integrated along the zero-order characteristic lines (10), as follows:

$$j\omega f_{1c}(\mathbf{P}_0,z,\omega)+\frac{P_{0z}}{\gamma_0 m_0}\frac{\partial}{\partial z}f_{1c}+\mathbf{F}_{1c}\cdot\nabla_{p0}f_{0c}(\mathbf{P}_0)=0 \tag{11}$$

where $f_{0c}(\mathbf{P}_0)$ is the electron zero-order distribution function at the entrance to the interaction region ($z=0$). The first-order force induced by the transverse em fields along the characteristic lines is given by

$$\mathbf{F}_{1c}=-e\left(\mathbf{E}_\perp+\frac{P_{cz}\mu_0}{\gamma_0 m_0}\hat{\mathbf{z}}\times\mathbf{H}_\perp+\frac{\mu_0}{\gamma_0 m_0}\mathbf{P}_{c\perp}\times\mathbf{H}_\perp+\hat{\mathbf{z}}E_z\right). \tag{12}$$

For a CRM interaction with a single circularly polarized wave, we assume a slowly varying wave amplitude $A(z)$ along the interaction region. The em wave propagating in the ferrite-loaded waveguide, in the region of the electron beam, is described by the transverse components of the wave equation (1) as

$$\mathbf{H}_\perp=\pm jA(z)\hat{\mathbf{e}}^{\pm}\hat{\phi}_H^{\pm}H_0e^{-j\beta z}, \tag{13a}$$

$$\mathbf{E}_\perp=A(z)\hat{\mathbf{e}}^{\pm}\hat{\phi}_E^{\pm}H_0Z_a^{\pm}e^{-j\beta z}, \tag{13b}$$

and by the axial component of the electric field $E_z = A(z)\hat{\phi}_{Ez}^{\pm} E_{z0} e^{-j\beta z}$, where $+/-$ denote a right-left-hand polarization, and $\hat{\mathbf{e}}^{\pm} = \hat{\mathbf{x}} \mp j\hat{\mathbf{y}}$ is the circularly polarized unit vector. The transverse profiles of the em mode are $\hat{\phi}_H^{\pm}$, $\hat{\phi}_E^{\pm}$, and $\hat{\phi}_{Ez}^{\pm}$ (note that within the *e*-beam cross section $\hat{\phi}_H^{\pm} \approx \hat{\phi}_E^{\pm}$). The initial transverse magnetic field is H_0, and E_{z0} is the initial axial electric field. The longitudinal wave number β is found as described in Sec. II A above.

Assuming a uniform initial azimuthal distribution of the electron beam, the distribution function $f_{0c}(\mathbf{P}_0)$ is independent of ψ_0. Consequently, $\partial f_{0c}/\partial P_{0x} = (\partial f_{0c}/\partial P_{0\perp})\cos\psi$, $\partial f_{0c}/\partial P_{0y} = (\partial f_{0c}/\partial P_{0\perp})\sin\psi$, and the Vlasov equation (11) is rewritten in the form

$$
\begin{aligned}
&j\omega f_{1c}(\mathbf{P}_0, z, \omega) + \frac{P_{0z}}{\gamma_0 m_0}\frac{\partial}{\partial z} f_{1c} \\
&\quad = e\left[\left(Z_a^{\pm} - \frac{P_{0z}\mu_0}{\gamma_0 m_0}\right)\frac{\partial f_{0c}}{\partial P_{0\perp}} + \frac{P_{0\perp}\mu_0}{\gamma_0 m_0}\frac{\partial f_{0c}}{\partial P_{0z}}\right] \\
&\qquad \times A(z)\hat{\phi}_H^{\pm} H_0 e^{-j(\beta z \pm k_c z \pm \psi_0)} \\
&\qquad + e\frac{\partial f_{0c}}{\partial P_{0z}} A(z)\hat{\phi}_{Ez}^{\pm} E_{z0} e^{-j\beta z}. \qquad (14)
\end{aligned}
$$

Substituting Eq. (13) into the wave equation (1), subtracting the homogeneous components [which do not include derivatives of $A(z)$ and are therefore equal to zero], and neglecting second derivatives of $A(z)$, we obtain the wave equation for the *e*-beam region ($r < r_b$)

$$
\pm 2\beta \frac{dA(z)}{dz}\hat{\mathbf{e}}^{\pm}\hat{\phi}_H^{\pm} H_0 e^{-j\beta z} = -\frac{\partial}{\partial z}(\hat{\mathbf{z}}\times\mathbf{J}_\perp) + \hat{\mathbf{z}}\times\boldsymbol{\nabla}_\perp J_z. \quad (15)
$$

Equations (9), (14), and (15) form a linear set of partial differential equations. In order to solve them, we apply the Laplace transform on the z dimension, $\tilde{A}(s) = \int_z A(z)e^{-sz}dz$, and rewrite Eqs. (9), (14), and (15) in the s domain as follows. The current components (9) are transformed to

$$
\begin{aligned}
\tilde{\mathbf{J}}_\perp(s,\omega) = -\frac{e}{2m_0}\int\int\int_{\mathbf{P}_0}\frac{P_{0\perp}}{\gamma_0}[&e^{j\psi_0}\tilde{f}_{1c}(s - jk_c)\hat{\mathbf{e}}^{+} \\
&+ e^{-j\psi_0}\tilde{f}_{1c}(s + jk_c)\hat{\mathbf{e}}^{-}]d^3\mathbf{P}_0 \qquad (16a)
\end{aligned}
$$

and

$$
\tilde{J}_z(s,\omega) = -\frac{e}{m_0}\int\int\int_{\mathbf{P}_0}\frac{P_{0z}}{\gamma_0}\tilde{f}_{1c}(s)d^3\mathbf{P}_0, \qquad (16b)
$$

where the first-order distribution function is given by the solution of the transformed first-order Vlasov equation (14) as follows:

$$
\begin{aligned}
\tilde{f}_{1c}(\mathbf{P}_0, s, \omega) = e&\left(j\omega + \frac{P_{0z}}{\gamma_0 m_0}s\right)^{-1} \\
&\times\left\{\left[\left(Z_a^{\pm} - \frac{P_{0z}\mu_0}{\gamma_0 m_0}\right)\frac{\partial f_{0c}}{\partial P_{0\perp}} + \frac{P_{0\perp}\mu_0}{\gamma_0 m_0}\frac{\partial f_{0c}}{\partial P_{0z}}\right]\right. \\
&\times\tilde{A}(s + j\beta \pm jk_c)e^{\mp j\psi_0}\hat{\phi}_H^{\pm} H_0 \\
&\left. + \frac{\partial f_{0c}}{\partial P_{0z}}\tilde{A}(s + j\beta)\hat{\phi}_{Ez}^{\pm} E_{z0}\right\}. \qquad (17)
\end{aligned}
$$

The wave equation (15) is transformed to

$$
\begin{aligned}
\pm 2\beta[(s + j\beta)\tilde{A}(s + j\beta) - A_0]\hat{\mathbf{e}}^{\pm}\hat{\phi}_H^{\pm} H_0 &= -s[\hat{\mathbf{z}}\times\tilde{\mathbf{J}}_\perp(s,\omega)] \\
&+ \hat{\mathbf{z}}\times\boldsymbol{\nabla}_\perp\tilde{J}_z(s,\omega), \qquad (18)
\end{aligned}
$$

where A_0 is the wave amplitude at the entrance ($z = 0$).

Substituting the distribution function (17) into the current components (16a),(16b) yields the expressions

$$
\begin{aligned}
\tilde{\mathbf{J}}_\perp^{\pm}(s,\omega) \cong -\frac{\pi e^2}{m_0}&\tilde{A}(s + j\beta)\hat{\mathbf{e}}^{\pm}\hat{\phi}_H^{\pm} H_0 \\
&\times\int_{P_{0z}}\int_{P_{0\perp}}\frac{P_{0\perp}}{\gamma_0}\left(j\omega + \frac{P_{0z}}{\gamma_0 m_0}s \mp \frac{j\omega_{c0}}{\gamma_0}\right)^{-1} \\
&\times\left[\left(Z_a^{\pm} - \frac{P_{0z}\mu_0}{\gamma_0 m_0}\right)\frac{\partial f_{0c}}{\partial P_{0\perp}} + \frac{P_{0\perp}\mu_0}{\gamma_0 m_0}\frac{\partial f_{0c}}{\partial P_{0z}}\right] \\
&\times P_{0\perp} dP_{0\perp} dP_{0z} \qquad (19a)
\end{aligned}
$$

and

$$
\begin{aligned}
\tilde{J}_z^{\pm}(s,\omega) \cong -\frac{2\pi e^2}{m_0}&\tilde{A}(s + j\beta)\hat{\phi}_{Ez}^{\pm} E_{z0} \\
&\times\int_{P_{0z}}\int_{P_{0\perp}}\frac{P_{0z}}{\gamma_0}\left(j\omega + \frac{P_{0z}}{\gamma_0 m_0}s\right)^{-1} \\
&\times\frac{\partial f_{0c}}{\partial P_{0z}} P_{0\perp} dP_{0\perp} dP_{0z}, \qquad (19b)
\end{aligned}
$$

where terms independent of ψ_0 vanish in the integration.

We assume now that the dominant poles are located in the s plane in the vicinity of the cyclotron-resonance condition; hence

$$
\left|j\omega + \frac{P_{0z}}{\gamma_0 m_0}s \mp \frac{j\omega_{c0}}{\gamma_0}\right| \sim 0, \qquad (20)
$$

where the $-/+$ signs correspond to the normal and anomalous modes of the CRM interaction, respectively. Sideband harmonics and other off-resonance effects that do not satisfy Eq. (20) are negligible. In particular, the axial current $\tilde{J}_z$ [Eq. (19b)], associated with the traveling-wave tube or Cerenkov

axial bunching effect, is off resonance in the CRM resonance condition (20) and therefore negligible [note that $V_{0z} \approx (\omega - \omega_c)/\beta$ is much smaller than the em phase velocity $V_{ph} = \omega/\beta$, and thus the denominator of Eq. (19b) exceeds the order of ω_c]. Therefore, even if $|E_z| \lesssim |\mathbf{E}_\perp|$ the effect of J_z is negligible with respect to $\mathbf{J}_\perp$ near the cyclotron resonance.

After integration by parts and some further algebraic steps, Eq. (19a) results in

$$\tilde{\mathbf{J}}_\perp^{\pm}(s,\omega) \cong \tilde{A}(s+j\beta)\hat{\mathbf{e}}^{\pm}\hat{\phi}_H^{\pm}H_0\frac{2\pi e^2}{m_0}\int_{P_{0z}}\int_{P_{0\perp}}\frac{1}{\gamma_0}\left[\left(j\omega+\frac{P_{0z}}{\gamma_0 m_0}s\mp\frac{j\omega_{c0}}{\gamma_0}\right)^{-1}\left(Z_a^{\pm}-\frac{P_{0z}\mu_0}{\gamma_0 m_0}\right)-\frac{1}{2}\left(j\omega+\frac{P_{0z}}{\gamma_0 m_0}s \mp\frac{j\omega_{c0}}{\gamma_0}\right)^{-2}\left(\frac{P_{0\perp}}{\gamma_0 m_0}\right)^2\left(\frac{j\omega}{c^2}Z_a^{\pm}+s\mu_0\right)\right]f_{0c}P_{0\perp}\,dP_{0\perp}\,dP_{0z}. \tag{21}$$

In the ideal case of a cold and azimuthally uniform electron beam, the zero-order electron distribution on axis is approximated by

$$f_{0c}(\mathbf{P}_0) \cong \frac{n_0}{2\pi\overline{P}_{0\perp}}\delta(P_{0\perp}-\overline{P}_{0\perp})\,\delta(P_{0z}-\overline{P}_{0z}), \tag{22}$$

where n_0 is the electron density and δ is a Dirac function. We substitute the current equation (21) in the ideal limit (22) into the wave equation (18). In the region of the electron beam $Z_a^{\pm} = V_{ph}^{\pm}\mu_0$, where $V_{ph}^{\pm}$ is the em phase velocity of the homogeneous solution. The above results in

$$\begin{aligned}-2j\beta[(s+j\beta)\tilde{A}(s+j\beta)-A_0] &= \frac{\omega_p^2}{c^2}F_f\left[\frac{s}{j(\omega\mp\omega_c)+s\overline{V}_{0z}}(V_{ph}^{\pm}-\overline{V}_{0z})\right. \\ &\quad \left.-\frac{\overline{V}_{0\perp}^2}{2}\frac{s}{[j(\omega\mp\omega_c)+s\overline{V}_{0z}]^2}\left(\frac{j\omega}{c^2}V_{ph}^{\pm}+s\right)\right] \\ &\quad \times\tilde{A}(s+j\beta),\end{aligned} \tag{23}$$

where $\omega_p = \sqrt{e^2 n_0/\gamma_0 m_0 \varepsilon_0}$ is the plasma angular frequency, F_f is the *e*-beam filling factor (8) for the fundamental em mode, and $\overline{V}_{0z} = \overline{P}_{0z}/\gamma_0 m_0$ and $\overline{V}_{0\perp} = \overline{P}_{0\perp}/\gamma_0 m_0$ are the average electron axial and perpendicular velocity components, respectively. This yields

$$\begin{aligned}-2j\beta[s\tilde{A}(s)-A_0] &= \frac{1}{c}\omega_p^2 F_f\frac{s-j\beta}{j(\omega\mp\omega_c)+(s-j\beta)\overline{V}_{0z}} \\ &\quad \times\left[(\overline{\beta}_{ph}^{\pm}-\overline{\beta}_{0z})-\frac{1}{2}\overline{\beta}_{0\perp}^2\frac{j\omega\overline{\beta}_{ph}^{\pm}+(s-j\beta)c}{j(\omega\mp\omega_c)+(s-j\beta)\overline{V}_{0z}}\right] \\ &\quad \times\tilde{A}(s),\end{aligned} \tag{24}$$

where $\overline{\beta}_{0z} = \overline{V}_{0z}/c$, $\overline{\beta}_{0\perp} = \overline{V}_{0\perp}/c$, and $\overline{\beta}_{ph}^{\pm} = V_{ph}^{\pm}/c$ are the normalized electron and phase velocity components.

The dimensionless operating parameters of the ferrite-guided CRM interaction are defined as follows. The tuning parameter is

$$\hat{\theta}^{\mp} = (\omega\mp\omega_c-\beta\overline{V}_{0z})\frac{L}{\overline{V}_{0z}} \tag{25}$$

where L is the interaction length. The normalized space-charge parameter is $\hat{\theta}_p = \omega_p L/\overline{V}_{0z}$, and the dimensionless wave number variables are $\hat{s} = jsL$, $\hat{k} = kL$, and $\hat{\beta} = \beta L$. This notation leads to a simplified gain-dispersion relation for the ferrite-guided CRM interaction as in Ref. [12]:

$$\tilde{A}(\hat{s}) = \frac{(\hat{s}-\hat{\theta}^{\mp})^2}{\hat{s}(\hat{s}-\hat{\theta}^{\mp})^2-\kappa(\hat{s})F_f C(\hat{s})\hat{\theta}_p^2}A_0, \tag{26}$$

where the coupling term for the circularly polarized wave in the ferrite-guided CRM is

$$\begin{aligned}\kappa(\hat{s}) &= \overline{\beta}_{0z}(\hat{s}-\hat{\theta}^{\mp})(\overline{\beta}_{ph}^{\pm}-\overline{\beta}_{0z}) \\ &\quad -\frac{1}{2}\overline{\beta}_{0\perp}^2(\hat{s}+\hat{\beta}-\hat{k}\overline{\beta}_{ph}^{\pm}),\end{aligned} \tag{27}$$

and the ratio parameter $C(\hat{s}) = (\hat{s}+\hat{\beta})/2\hat{\beta}$ is close to $\frac{1}{2}$ for slow waves. The resulting Pierce-type equation (26) for the ferrite-guided CRM interaction with a single circularly polarized mode is solved for several representative cases to demonstrate the ferrite effect in the next section.

III. FERRITE-CRM TUNABILITY

The unique feature of the ferrite-loaded waveguide stems from the dependence of its dispersion relation on the induced external magnetic field. This effect is shown for instance in Fig. 5 for the parameters listed in Table I. The dependence of the dispersion relation on the magnetic field enables one to vary the waveguide mode cutoff frequency, and to shift its entire dispersion curve according to the axial static magnetic field. Figure 5 shows, for instance, the variation in the dispersion relation of the right-hand circularly polarized mode (denoted ''1b'' in Fig. 2) for three values of the external

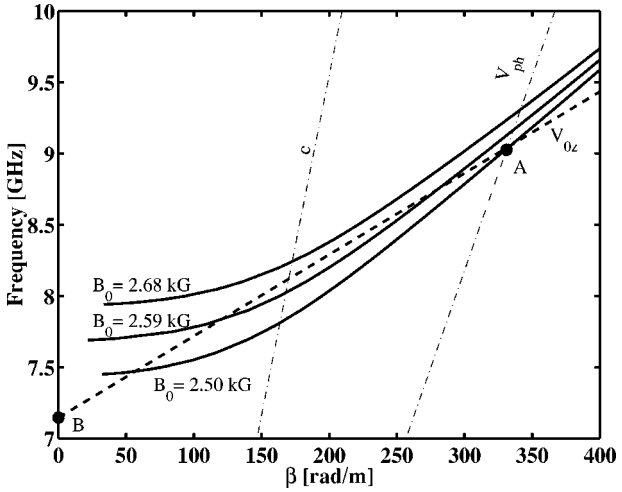

FIG. 5. The dispersion relation of the right-hand circularly polarized mode denoted ''1b'' in Fig. 2 for three values of the external magnetic field, $B_0=2.50$, 2.59, and 2.68 kG. The dashed line shows the electron beam line for the operating parameters of Table I with $B_0=2.5$ kG and $V_{eb}=7.5$ kV. Points *A* and *B* denote the CRM interaction point and the cyclotron frequency, respectively. The dotted lines present the em phase velocity slope V_{ph} and the free-space slope c ($V_{0z}=0.12c$ and $V_{ph}=0.57c$).

magnetic field (2.50, 2.59, and 2.68 kG). An increase of B_0 by 0.09 kG leads to an increase of 0.25 GHz in the ferrite resonance frequency, and consequently to a similar increase of the waveguide cutoff frequency. Hence, in the ferrite-loaded CRM, the frequency range can be tuned not only by varying the *e*-beam energy but also by using the axial magnetic field effect on the ferrite. Here, the magnetic field affects not only the electron-cyclotron frequency (as in an ordinary CRM), but also the ferrite resonance frequency and consequently the spectral response of the waveguide.

Figure 5 shows, for instance, the *e*-beam line for $B_0=2.5$ kG, $V_{eb}=7.5$ kV, and the other parameters listed in Table I. The CRM interaction with the corresponding em wave is denoted as point *A* in this dispersion diagram. The phase velocity at this point is $0.57c$, whereas the electron axial velocity is $0.12c$, and hence the two are intentionally mismatched ($V_{ph}\sim 5V_{0z}$).

The tunability feature of the ferrite-loaded CRM device is demonstrated in this section by a numerical example. The gain-dispersion relation (26) is solved by an inverse Laplace transform of $\tilde{A}(\hat{s})$ for the parameters listed in Table I. Figure 6 shows gain curves of the CRM interaction in three different *e*-beam voltages (6.5, 7.5, and 8.5 kV) for the same static magnetic field (2.59 kG). This tuning effect, by varying the electron energy, is similar in principle to the ordinary CRM. But in a ferrite-guided CRM a variation in the static magnetic field leads to a wider tunability range because of the ferrite response to this field. Figure 7 demonstrates this feature by three gain curves of the CRM interaction in different magnetic fields (2.50, 2.59, and 2.68 kG) for the same *e*-beam voltage (7.5 kV). The instantaneous bandwidth is ~ 0.3 GHz and the tunability range attains 1.2 GHz in this example.

It should be noted that this CRM performance in such a low operating voltage is not achievable in an empty waveguide of the same diameter (16 mm), because its cutoff frequency (11 GHz) is higher than that of the ferrite-loaded waveguide (7.5 GHz).

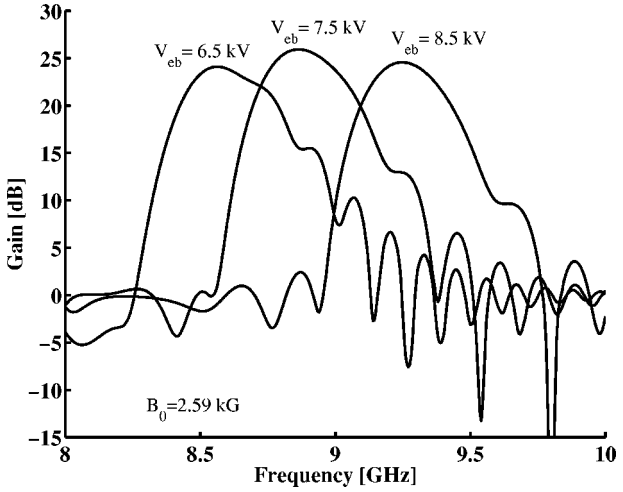

FIG. 6. Gain vs frequency for $B_0=2.59$ kG, and *e*-beam voltages of 6.5, 7.5, and 8.5 kV, for the parameters listed in Table I.

IV. DISCUSSION

The concept of a ferrite-guided CRM is proposed and discussed theoretically in this paper. The ferrite medium slows the em wave and enhances its magnetic field component. This enables a CRM interaction in the Weibel regime, in which the axial bunching mechanism is dominant. The ferrite-guided CRM may also attain the anomalous Doppler condition (with the left-hand circular polarization modes).

A linear gain dispersion equation (26) is derived in this paper using the formalism of Ref. [12], whereas the ferrite-loaded waveguide parameters (i.e., the wave number, phase velocity, impedance, and filling factor) are found numerically according to Ref. [18]. Unlike in an ordinary CRM, the

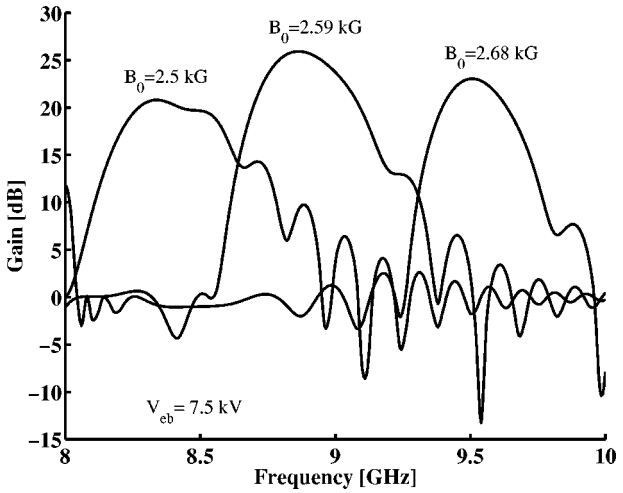

FIG. 7. Gain vs frequency for *e*-beam voltage of 7.5 kV, and external magnetic fields of 2.50, 2.59, and 2.68 kG, for the parameters listed in Table I.

waveguide parameters depend on the axial-magnetic field strength, which adds another dimension of tunability to this CRM scheme. The gain vs frequency of the ferrite-guided CRM amplifier is calculated numerically for several examples to demonstrate this tunability feature.

The slow-wave interaction widens the spectral bandwidth of the amplification curve, but unlike dielectric-loaded CRM schemes, the spectral response of the ferrite guide depends on the induced magnetic field, and it can be made selective in frequency. For instance, the losses associated with the ferrite resonance frequency (which differs from the CRM operating frequency by the Doppler shift and is therefore neglected in this study) can be utilized in future schemes to suppress selectively backward waves and other spurious oscillations. This may extend the concept demonstrated by Chu *et al.* [5] with a resistive load. In future schemes, ferrite components can be incorporated within CRM tubes as internal phase shifters to enhance gain and efficiency. Ferrite-guided CRM's can be made in rectangular and planar shapes as well.

Further theoretical and experimental studies are needed following this conceptual study in order to evaluate the features of the ferrite-guided CRM's and to examine their characteristics. These include nonlinear analysis in a wide range of parameters, taking into account multimode transverse effects and ferrite losses. An experimental demonstration of the ferrite-loaded CRM concept is considered in [19].

[1] V. L. Granatstein and I. Alexeff, *High-Power Microwave Sources* (Artech House, Boston, 1987), and references therein.
[2] K. R. Chu and J. L. Hirshfield, Phys. Fluids **21**, 461 (1978).
[3] For a recent update, see M. Thumm, Forschungszentrum Karlsruhe, Technik und Umwelt Wissenschaftliche Berichte Report No. FZKA 6588, 2001 (unpublished).
[4] T. Idehara, T. Tatsukawa, S. Matsumoto, K. Kunieda, K. Hemmi, and T. Kanemaki, Phys. Lett. A **132**, 344 (1988).
[5] K. R. Chu, H. Y. Chen, C. L. Hung, T. H. Chang, L. R. Barnett, S. H. Chen, T. T. Yang, and D. J. Dialetis, IEEE Trans. Plasma Sci. **27**, 391 (1999).
[6] H. Guo, L. Chen, H. Keren, J. L. Hirshfield, S. Y. Park, and K. R. Chu, Phys. Rev. Lett. **49**, 730 (1982).
[7] M. Einat and E. Jerby, Phys. Rev. E **56**, 5996 (1997).
[8] E. Jerby and G. Bekefi, Phys. Rev. E **48**, 4637 (1993).
[9] E. Jerby, A. Shahadi, V. Grinberg, V. Dichtiar, E. Agmon, H. Golombek, V. Trebich, M. Bensal, and G. Bekefi, IEEE J. Quantum Electron. **31**, 970 (1995).
[10] B. I. Ivanov, D. V. Gorozhanin, and V. A. Miroshnichenko, Pis'ma Zh. Tekh. Fiz. **5**, 1112 (1979) [Sov. Tech. Phys. Lett. **5**, 464 (1979)].
[11] A. N. Didenko, A. R. Borisov, G. P. Fomenko, A. S. Shlapakovskii, and YuG. Shtein, Pis'ma Zh. Tekh. Fiz. **9**, 1331 (1983) [Sov. Tech. Phys. Lett. **9**, 572 (1983)].
[12] E. Jerby, Phys. Rev. E **49**, 4487 (1994).
[13] E. Jerby (unpublished).
[14] A. W. Trivelpiece, A. Ignatius, and P. C. Holscher, J. Appl. Phys. **32**, 259 (1961).
[15] J. Spector and A. W. Trivelpiece, J. Appl. Phys. **35**, 2030 (1964).
[16] R. Chatterjee, *Advanced Microwave Engineering Special Advanced Topics* (Ellis Horwood Publishers, Chichester, England, 1988).
[17] R. E. Collin, *Foundations for Microwave Engineering* (McGraw-Hill, New York, 1992).
[18] A. J. Baden Fuller, Proc. Inst. Electr. Eng. **108C**, 339 (1961).
[19] E. Jerby *et al.* (unpublished).